Development of a surface feature motion estimation system for the Gulf of St. Lawrence using SST images

P. Larouche, J.-M. Boucher and É. Thomassin

Ocean Sciences Branch
Fisheries and Oceans Canada
Maurice Lamontagne Institute
P.O. Box 1000, 850, route de la Mer
Mont-Joli, Québec
G5H 3Z4 Canada

2006

Canadian Technical Report of Hydrography and Ocean Sciences 250

Canadian Technical Report of Hydrography and Ocean Sciences

Technical reports contain scientific and technical information of a type that represents a contribution to existing knowledge but which is not normally found in the primary literature. The subject matter is generally related to programs and interests of the Oceans and Science sectors of Fisheries and Oceans Canada.

Technical reports may be cited as full publications. The correct citation appears above the abstract of each report. Each report is abstracted in the data base *Aquatic Sciences and Fisheries Abstracts.*

Technical reports are produced regionally but are numbered nationally. Requests for individual reports will be filled by the issuing establishment listed on the front cover and title page.

Regional and headquarters establishments of Ocean Science and Surveys ceased publication of their various report series as of December 1981. A complete listing of these publications and the last number issued under each title are published in the *Canadian Journal of Fisheries and Aquatic Sciences*, Volume 38: Index to Publications 1981. The current series began with Report Number 1 in January 1982.

Rapport technique canadien sur l'hydrographie et les sciences océaniques

Les rapports techniques contiennent des renseignements scientifiques et techniques qui constituent une contribution aux connaissances actuelles mais que l'on ne trouve pas normalement dans les revues scientifiques. Le sujet est généralement rattaché aux programmes et intérêts des secteurs des Océans et des Sciences de Pêches et Océans Canada.

Les rapports techniques peuvent être cités comme des publications à part entière. Le titre exact figure au-dessus du résumé de chaque rapport. Les rapports techniques sont résumés dans la base de données *Résumés des sciences aquatiques et halieutiques*.

Les rapports techniques sont produits à l'échelon régional, mais numérotés à l'échelon national. Les demandes de rapports seront satisfaites par l'établissement auteur dont le nom figure sur la couverture et la page de titre.

Les établissements de l’ancien secteur des Sciences et Levés océaniques dans les régions et à l'administration centrale ont cessé de publier leurs diverses séries de rapports en décembre 1981. Vous trouverez dans l'index des publications du volume 38 du *Journal canadien des sciences halieutiques et aquatiques*, la liste de ces publications ainsi que le dernier numéro paru dans chaque catégorie. La nouvelle série a commencé avec la publication du rapport numéro 1 en janvier 1982.

Canadian Technical Report of
Hydrography and Ocean Sciences 250

2006

DEVELOPMENT OF A SURFACE FEATURE MOTION ESTIMATION SYSTEM FOR THE GULF OF ST. LAWRENCE USING SST IMAGES

By

P. Larouche, J.-M. Boucher[1] and É. Thomassin[1]

Ocean Sciences Branch
Fisheries and Oceans Canada
Maurice Lamontagne Institute
P.O. Box 1000, 850, route de la Mer
Mont-Joli (Québec) G5H 3Z4
LaroucheP@dfo-mpo.gc.ca

[1] GET, ENST Bretagne, FRE CNRS TAMCIC, CS 8381, 29238 Brest Cedex 3, France

Cat. Number Fs 97-18/250E ISSN 1488-5417

Correct citation for this publication:

Larouche, P., J.-M. Boucher and É. Thomassin. 2006. Development of a surface feature motion estimation system for the Gulf of St. Lawrence using SST images. Can. Tech. Rep. Hydrogr. Ocean Sci. 250: iii + 21pp.

ABSTRACT

Larouche, P., J.-M. Boucher and É. Thomassin, 2006. Development of a surface feature motion estimation system for the Gulf of St. Lawrence using SST images. Can. Tech. Rep. Hydrogr. Ocean Sci. 250: iii + 21pp.

We present an image processing system to evaluate sea surface feature motion using pairs of sequential sea surface temperature images. The system uses a set of filters to produce the best possible tracers and a combination of shape-matching and Hough transform to evaluate tracer motion. A set of optimal parameters was defined, balancing the number of vectors produced and their quality for the Gulf of St. Lawrence region. This set was used to process 19 image pairs representing diverse time intervals and seasons. When false vectors generated by clouds were eliminated, approximately 50% of the calculated displacement vectors were of good quality. This could be improved but at the detriment of the number of vectors. The best results are obtained when the images are separated by only one satellite orbital period.

RÉSUMÉ

Larouche, P., J.-M. Boucher and É. Thomassin. 2006. Development of a surface feature motion estimation system for the Gulf of St. Lawrence using SST images. Can. Tech. Rep. Hydrogr. Ocean Sci. 250: iii + 21pp.

Nous présentons un système d'analyse d'images permettant d'évaluer le déplacement de traceurs en utilisant des paires d'images de température de surface de la mer. Des filtres sont utilisés pour générer les meilleurs traceurs et une combinaison de correspondance de forme et de transformée de Hough évalue le déplacement. Un ensemble de paramètres optimaux a été défini afin d'obtenir un équilibre entre le nombre de vecteurs obtenus et leur qualité pour le golfe du Saint-Laurent. Cet ensemble a été utilisé pour traiter 19 paires d'images représentant diverses saisons et intervalles de temps. Après élimination des faux vecteurs générés par les nuages, environ 50 % des vecteurs obtenus étaient de bonne qualité. Ceci pourrait être amélioré mais au détriment du nombre de vecteurs. Les résultats étaient meilleurs lorsque les images n'étaient séparées que d'une période orbitale du satellite.

1.0 INTRODUCTION

Surface currents are one of the most important dynamic features of the world ocean, transporting heat, nutrients and organisms. It is thus important to evaluate their characteristics. Typically, oceanographers are interested in measuring the speed and direction of the surface layer over broad areas to detect the presence of coastal currents, gyres and other dynamic features important to an ecosystem. Unfortunately, due to the presence of waves, the precise measurement of surface currents is almost impossible to accomplish using traditional measuring devices such as current meters. Surface drifters can provide information but are limited both spatially and temporally. Oceanographers thus started using remote sensing information to evaluate surface currents. Different techniques can be used to accomplish this, such as satellite altimetry, direct measurement of speed by radar interferometry and coastal radars. Another satellite-based approach is the use of sequential images to track ocean features. The type of information generally used in this process is sea surface temperature (SST) images produced from meteorological satellite data, but other data sources such as ocean colour images can also be used (Boxall and Robinson 1987; Svejkovsky 1988; Garcia and Robinson 1989; Tokmakian et al. 1990; Hedger et al. 2001).

The Gulf of St. Lawrence is a coastal sea located in eastern Canada that is characterized by a large influence of tides and freshwater and for which data on surface currents is mostly limited to a few drifter experiments in the estuarine portion. Satellite imagery could thus provide information on mesoscale surface currents that would then be suitable for a variety of applications. The motion of surface features is not necessarily directly representative of the instantaneous surface current. This is particularly true in areas where strong baroclinic fields exist for which the water moves along the isotherms. However, despite that limitation, numerous feature tracking experiments done in different coastal environments showed that this approach can provide current estimates that are consistent with other measurements made using current meters (Holland and Yan 1992; Yan and Breaker 1993; Vigan et al. 2000), drifting buoys (Emery et al. 1986; Holland and Yan 1992; Yan and Breaker 1993; Vigan et al. 2000), altimetric measurements (Bowen et al. 2002; Emery et al. 2004) or models (Emery et al. 1992). Feature tracking can thus provide useful information about the general circulation patterns even in areas affected by baroclinic fields or within rotational flows (Svejovsky 1988; Kelly and Strub 1992; Vastano and Barron 1994; Gao and Lythe 1998; Bowen et al. 2002) In these cases, it is believed that the presence of small cross-frontal features allows the evaluation of along-isotherm circulation (Domingues et al. 2000). The main limitations associated with the feature tracking approach are isothermal fields for which no gradients can be identified (Gao and Lythe 1998) and regions where non-advective processes dominate (Wahl and Simpson 1990; Domingues et al. 2000; Hedger et al. 2001). In the Gulf of St. Lawrence, the former is probably the most important, especially at the beginning and end of winter when the sea surface is free of ice and shows low temperatures everywhere. Non-advective processes (e.g., diffusion and mixing) affecting the horizontal SST field are potentially important in a few restricted areas, such as the estuarine portion, where relatively strong thermal gradients can be encountered. However, Wahl and Simpson (1990) indicated that diffusion is not a problem over the 1 to 10 km spatial scales and for images taken within 6-24 hours, even in strong thermal gradients. We thus decided to build a completely automated system that could process NOAA AVHRR data captured over the Gulf of St. Lawrence. The system needed to be efficient and capable of working with data of high

dynamic range as the seasonal cycle of water temperature is large in the Gulf. Moreover, we wanted to be able to verify the system performance in terms of accuracy. Our approach was thus to use a series of processes for which various parameters needed to be optimized in order to provide the best results. This report presents our achievements to date. Section 2 reports on the development of a system to identify ocean features. Section 3 deals with the estimation of motion and system implementation, and illustrates the overall system performance using a set of real data together with an evaluation of the quality of the produced vectors.

2.0 OCEAN FEATURE EXTRACTION

The first problem to solve in order to build a feature tracking system is the identification of features. To be detectable, features must have a signature that can be extracted from an image. On AVHRR images, oceanographic features are often associated with thermal gradients of varying intensities. However, since currents are driven both by changes in salinity and temperature, detection problems using AVHRR may occur in higher latitude regions where SST is almost constant over broad geographic areas for some periods of time. This is generally not a problem in the more temperate regions since strong thermal contrasts are almost always present. Methods must thus be found to identify more subtle features in SST images having a small dynamic range, such as in the Gulf of St. Lawrence in the spring and fall. Figure 1 shows the schematic representation of the image processing system developed for the St. Lawrence.

Ocean feature extraction is based on the notion that SST gradients are associated with *in situ* dynamic processes. Temperature maps produced using NOAA AVHRR data have a spatial resolution of approximately 1.1 km at nadir (Figure 2). Because of this relatively low spatial resolution, the images are often noisy, reflecting very small changes resulting from the nearest-neighbour resampling algorithm used to geometrically correct the images or from sub-pixel clouds that often go undetected by cloud detection algorithms.

To extract features, SST images are first transformed into gradient images. Since gradient filters are sensitive to noise, the navigated images are pre-processed using a median filter of size 3x3. Pursuant to this step, the spatial gradient is calculated to show all the potential features contained in the image. Our choice for this step was to use a size 3 Sobel filter. This choice was made over other filters such as the sigma filter (Lee 1984) and the cluster shade texture (Holyer and Peckinpaugh 1989) because the Sobel operator retains more of the fine structure present in the images. Our implementation of this filter includes the rejection of data in a band of 2 pixels around land and clouds that were previously masked (Figure 3).

The Sobel operator is based on two convolution filters (one horizontal and one vertical) used to calculate the gradient module (Eq. 1)

Horizontal filter (gx): $\begin{matrix} -1 & 0 & 1 \\ -2 & 0 & 2 \\ -1 & 0 & 1 \end{matrix}$ Vertical filter (gy): $\begin{matrix} -1 & -2 & -1 \\ 0 & 0 & 0 \\ 1 & 2 & 1 \end{matrix}$ (1)

$$Module = \sqrt{(gx)^2 + (gy)^2}$$

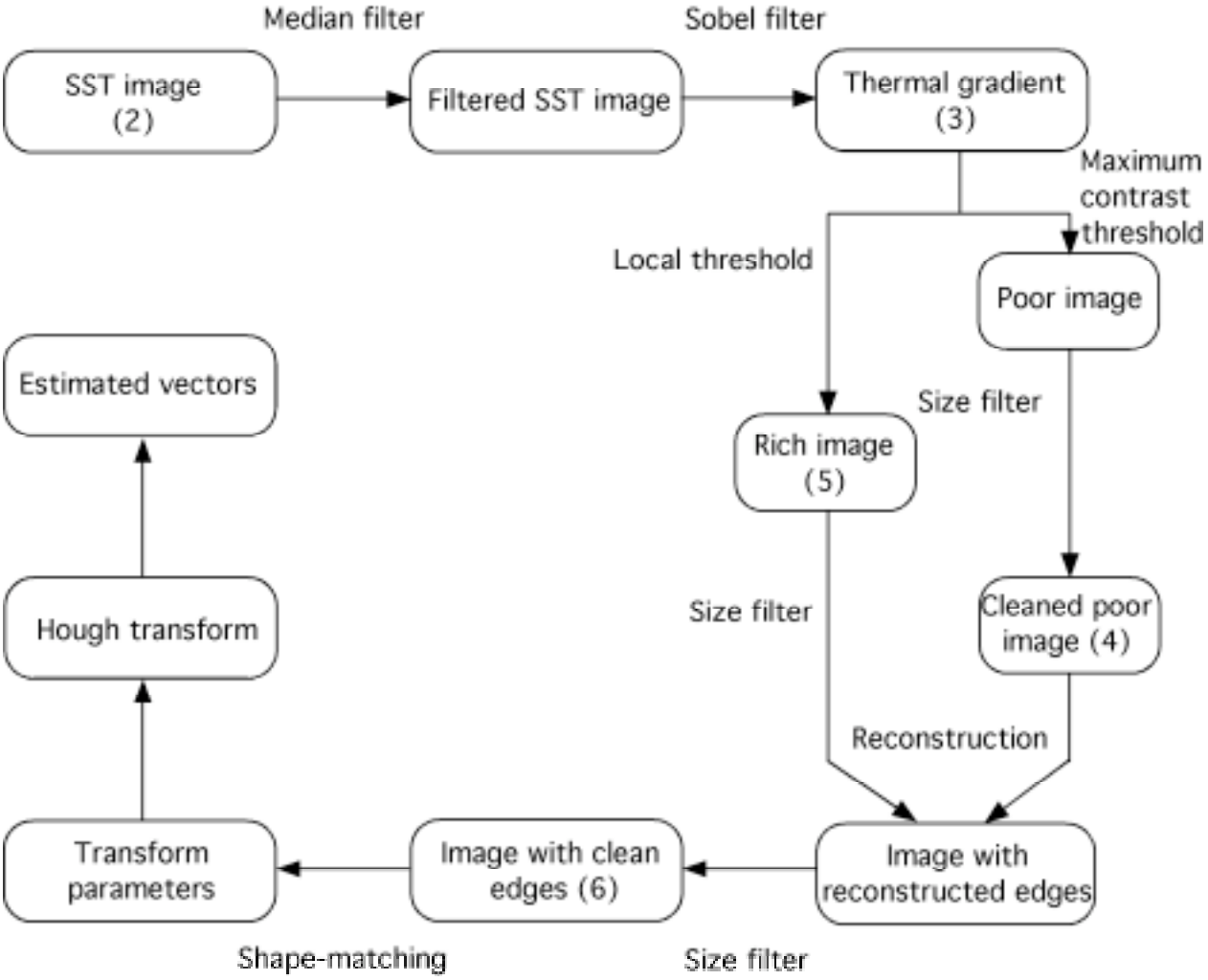

Figure 1. Schematic representation of the image processing system developed for the St. Lawrence. Numbers in parentheses refer to other figures in the report.

At this point, the gradient image contains a large amount of information of limited value for feature tracking and therefore must be further cleaned so it only retains the pertinent features. A few procedures have already been proposed to this end. The ordered statistical edge detection algorithm (OSEDA) filters edges using a criterion based on edge sharpness. This criterion is used for the entire processed image regardless of local dynamics, leading to an undersampling of the areas having less defined gradients. A more localized and flexible approach is thus needed in the context of an operational system. Such a procedure has recently been proposed using morphological operators that take into consideration local image dynamics (Krishnamurthy et al. 1994). Results show that this approach can detect either strong or weak gradients (distributed over 6-7 pixels) if the size of the structuring element is large enough (typically 21x21). As it generates edges that are generally thick, some post-processing is required to extract the true edge location that can then be used for motion analysis.

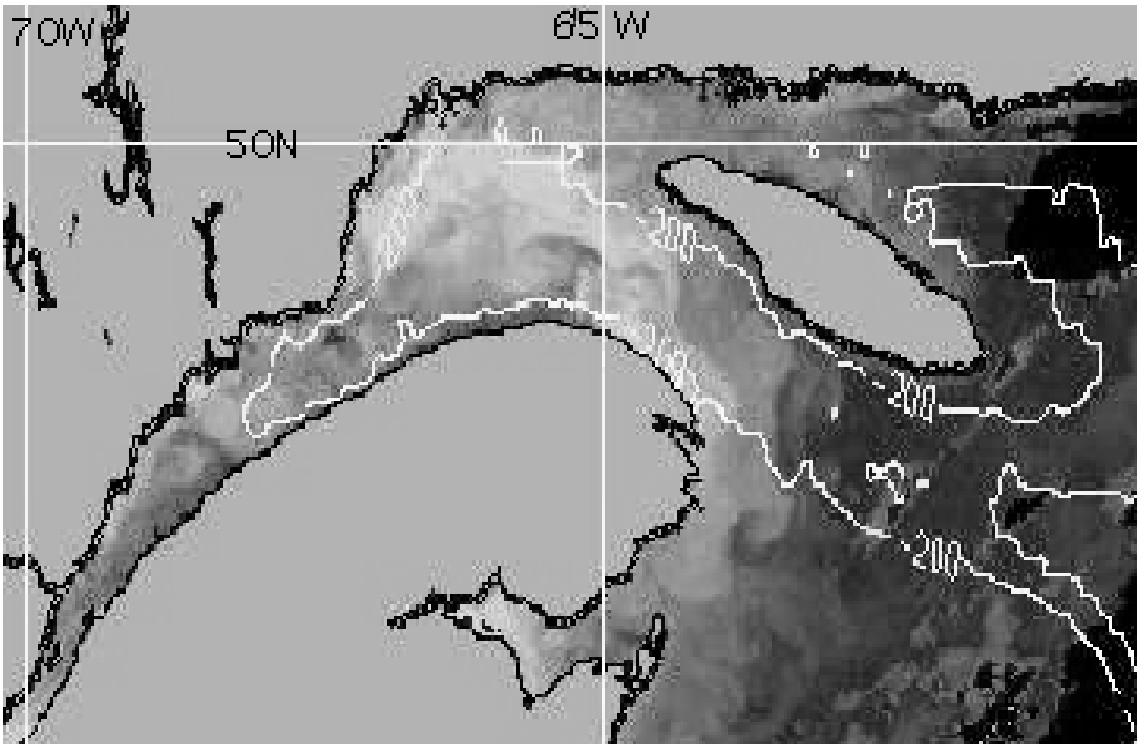

Figure 2. NOAA AVHRR channel 4 brightness temperature image of the Gulf of St. Lawrence with the 200 m isobath shown.

We thus looked for an alternative approach that could be applied to a broad range of SSTs, would be simple to implement and would produce information of good quality for the motion detection procedure. It will be shown that this last specification is the most important. It implies that the selected edges must have a low noise level and be as continuous as possible to prevent erroneous shape matches.

Edge detection requires finding an optimum filter. Using a too-selective filter will only retain strong gradients, leaving many gaps in the data, while a less selective filter will retain too much information, most of which will be undesirable. Our approach was thus to build a filtering system based on mathematical morphology that would take advantage of the different filters available to produce images of different richness (one rich, one poor) and then combine these two images to build the final image showing the cleaned edges.

The first step consists in applying a local threshold defined to maximize mean local contrast (Kohler 1981). This algorithm is based on the principle that true edges should have a relatively strong contrast within their local environment. The optimal threshold is thus the one that can detect the most high-contrast edges and the least low-contrast. Mean contrast is defined as the mean of the absolute differences between grey levels inside and outside the edge over a window of size (Tx1,Ty1). Applying this filter leads to an image from which most low contrast edges have been dismissed. To further clean this image, we eliminate remaining small aggregates with sizes less than K1 pixels, leading to a poor image containing only essential but incomplete

information (Figure 4). Gaps of size K2 are allowed in the calculation of aggregate size to take care of slightly fragmented edges.

The next step is then to generate the rich image by applying a local sill conserving only a fixed number of points (K3% having the higher grey levels) over a window size (Tx2,Ty2). Like the previous one, this filter has also been designed to take into account local image dynamics. As this filter generates noise in areas of low thermal gradients, a minimum size of K4 pixels is imposed for the resulting feature. The result is thus a rich image containing more features, some of which are useless (Figure 5).

These two images are then used to build a final clean-edge image by reconstructing the edges contained in the poor image using the information contained in the rich one. Edges in the poor image are thus completed by the addition of all adjacent edge points taken from the rich image, leading to less fragmented edges. The final step consists of the elimination of small aggregates of size less than K5 resulting from remaining noise in the poor image. However, to allow the conservation of slightly fragmented edges, gaps of 1 pixel are allowed in the calculation of the aggregate size. The final product can be seen in Figure 6.

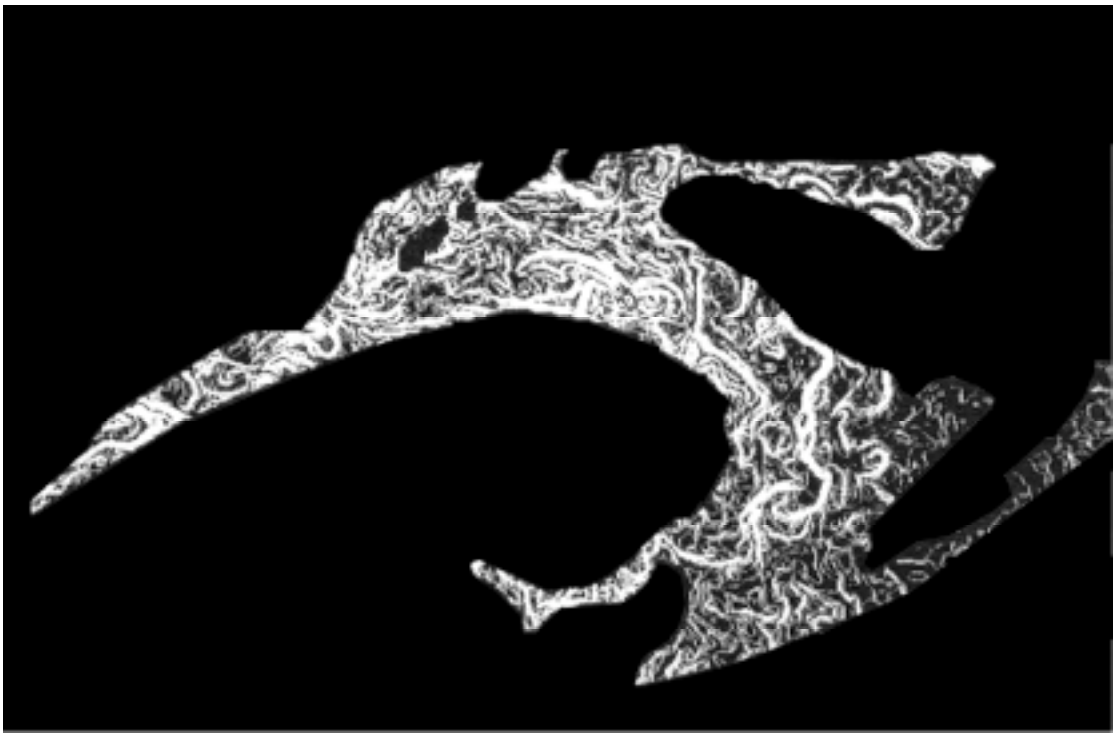

Figure 3. Gradient image using the Sobel operator.

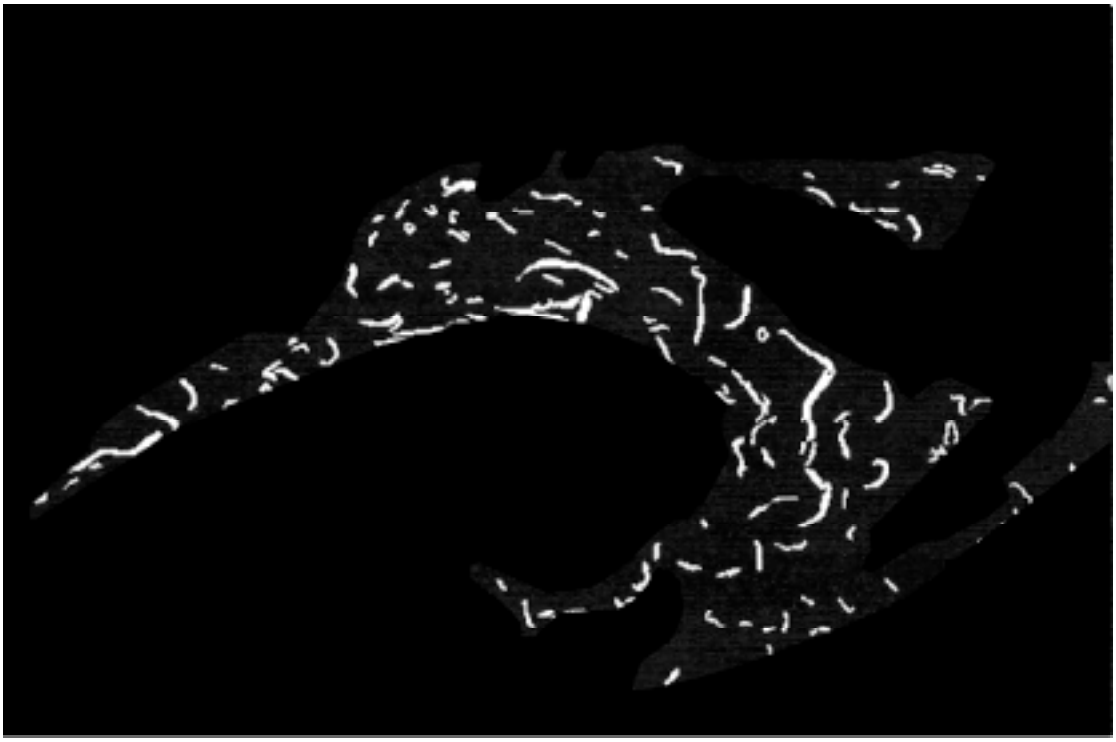

Figure 4. Poor image generated using the maximum local contrast filter and after further cleaning to eliminate small aggregates.

Figure 5. Rich image generated using the local sill filter and cleaned of its small aggregates.

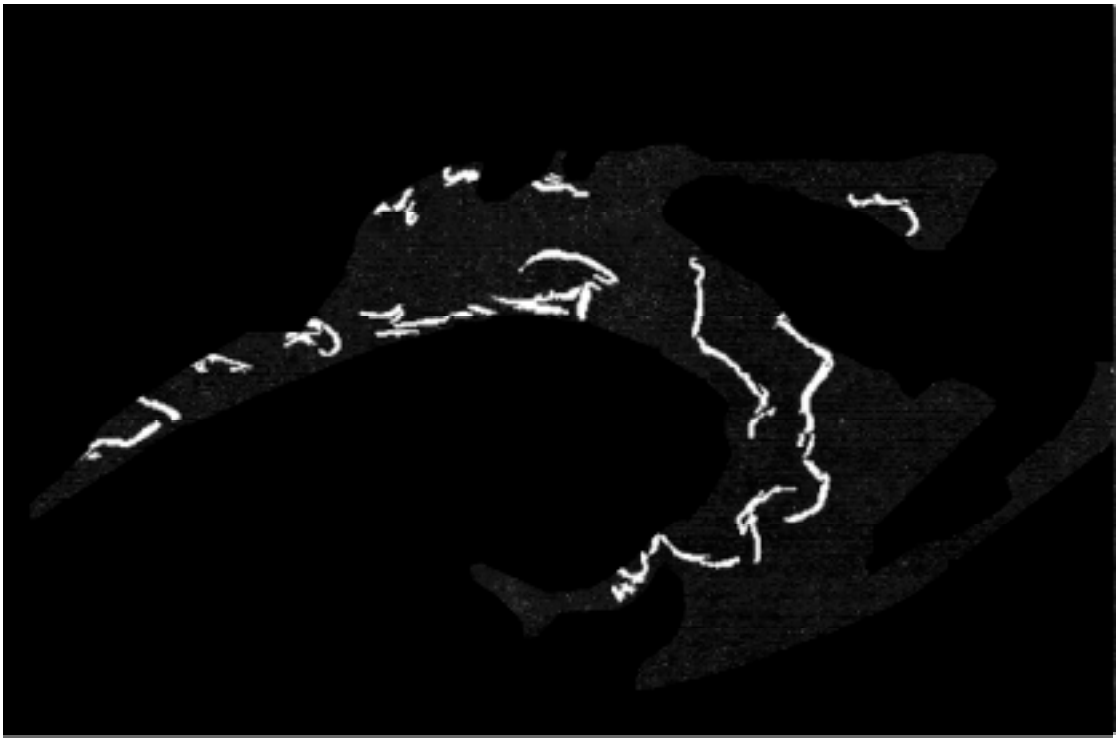

Figure 6. Features reconstructed using the poor and rich images and after removal of small aggregates.

3.0 MOTION ESTIMATION

There exist two common approaches to motion estimation. The first is based on the use of correlation methods and the second on feature tracking. In the correlation methods group, the most used and tested method is the maximum cross-correlation (MCC) technique originally developed for cloud tracking and first applied to oceanography by Emery et al. (1986). However, this method is limited only to translation motion and is computationally expensive. Different modifications to the method have been proposed to address these problems (Kamachi 1989; Yan and Breaker 1993; Leming 1994; Tonsmann et al. 2002). Another proposed correlation method is the use of SST images to solve the heat equation in the surface layer and determine the currents (Kelly 1989; Vigan et al. 2000). This method has been shown to produce results of the same quality as the MCC technique (Kelly and Strub 1992). Drawbacks of this method are the necessity to use the most accurate SST possible, which is currently on the order of 0.5°C, and the fact that the assumption of predominance of advection over diffusion does not hold in dynamic environments. Other correlation approaches based on the Hough transform can estimate rotation while shape-matching methods can also take care of edge deformation. The Hough transform approach has been tested using a few cases and was shown to match relatively well to known water velocities (Yan and Breaker 1993). However, because there are more unknowns than equations to solve both rotation and translation simultaneously, the method needs to use a two line correspondence approach assuming that both initial and target features would undergo the same translation and rotation. Finally, the shape-matching method was only tested using a very

limited set of well-defined thermal gradients in the Gulf Stream (Kuo and Yan 1994), so its overall performance is not totally quantified.

The second approach uses the tracking of individual features over time. This can either be accomplished by a human operator or by a computer software and has been mostly used in ice cover motion estimation (LaViolette and Hubertz 1975; Hatakeyama et al. 1985; Peterson 1987; Vastano and Barron 1994; Côté and Tatnall 1995; Thomas et al. 1995; Cho et al. 1998).

3.1 SYSTEM DESCRIPTION

As stated above, different tools are available to evaluate feature motion in successive image pairs. Published results seem to indicate that the Hough transform produces better results than the MCC technique. However, we believe that the two-line correspondence assumption used by Yan and Breaker (1993) to evaluate both rotation and translation may not always be valid in energetic systems where features can undergo deformations in a relatively short time. Our approach was thus to combine the strengths of both the shape-matching and Hough transform to estimate motion in the context of an operational system. The shape-matching is used as a first step to evaluate the rotation and sizing of the tracked feature that is then used by the Hough transform to evaluate translation in two-dimensional space. A complete mathematical description of the shape-matching method can be found in Kuo and Yan (1994). To ease interpretation of the results, the equations have been adapted to put the reference point in the center of the image instead of the upper left corner as defined in Kuo and Yan (1994). The processing starts from previously detected edges in two consecutive images and attempts to find the best possible match between them. The procedure cuts the first image into a series of small windows of size (Tx3, Ty3) that overlap by (Tx3/2, Ty3/2). A search zone of a larger size is then defined in the second image centered on the same coordinates as the reference point in the first image. This zone is then cut into search windows of size (Tx3, Ty3), but overlapping more than in the first image. A feature S' found in the search window is put into correspondence with the window located in the first image using the shape-matching approach. The window for which the maximum similarity is found is thus retained for further processing together with its estimated transformations. The feature motion will be the sum of the computed translation and the shift between the centers of the starting and search windows. If considered reliable, the estimated transformations are then stored in a file that will be used by the Hough transform in the second processing step.

The reliability is defined by the similarity between the true pattern S' (in the search window) and the pattern S (in the starting window) transformed using the evaluated translation, rotation and sizing, with a value of 1 being the best possible similarity. All the estimations for which the similarity coefficient falls within a given interval (K6) centered on this value will be considered reliable.

The shape-matching method is built upon the resolution of a linear system having four equations with four unknowns: rotation, x and y translation, and scaling. However, this system may be difficult to solve depending on the analyzed shapes. If the shapes are too symmetrical, the geometric centre and mean radius of each shape will be too close to each other. The system is thus ill conditioned and the classical solving algorithms used will generate an error during processing. To address this potential problem, the equation system is solved using a least-squares

method algorithm. For an ill-conditioned system, the results will be impossible (very high values) and will not be accepted. In other cases, results will be as precise as those obtained using classical solution methods.

In general, feature rotation should not exceed the defined domain (- /2, /2). Tests showed that some results were wrong because of bad matches having calculated rotations outside the defined domain. This can happen when small features having a limited number of points are matched to part of a larger form. To detect these bad matches, it was thus necessary to extend the definition domain to (- ,).

The second processing step is the use of the Hough transform to estimate motion between two consecutive images. The mathematical description of the Hough transform can be found in Yan and Breaker (1993). Since the main drawbacks of this algorithm are the problems of rotation and sizing, it is now possible to combine the results of the first processing step to increase the efficiency and precision of the Hough transform. As only good shape-matching results were selected during the first processing step, only a fraction of the original images has to be processed by the Hough algorithm thus increasing processing speed. The procedure reads the information contained in the file and transforms the feature contained in the starting tile for rotation and sizing. Then, the Hough transform finds the best translation of this feature in the search image. The calculated translation represents the movement of the feature between the center of the starting tile and the location of the maximum in the accumulator array weighted by the barycenter of a 3x3 window centered on the maximum. The barycenter is used because generally no clear peak exists in the accumulator array; there is rather a cluster of points around the maximum. The final result of both processing steps is a set of vectors that should reflect sea surface velocities. The reliability of the Hough transform is evaluated using the ratio (K7) between the maximum of the accumulation matrix and the number of edge points in the starting window. We also impose a minimum of K8 edge points within a window to process it.

3.2 SYSTEM IMPLEMENTATION

To implement the system, a series of tests were conducted to optimize the different parameters used in the edge generation process. Implementing feature tracking in an operational system is not an obvious task as many factors can decrease system performance. One of the most important is the framing of the tracked features. Most of the time, previous tests had been done using perfectly framed objects to evaluate motion estimation techniques. In practice, an automatic system will divide the images into a series of boxes that may very well split features in numerous parts, affecting the algorithm performance. Other factors such as the window and filter sizes may also influence the quality of the results. In order to evaluate the true performance of our proposed system, a series of tests was done to evaluate the quality of the calculated vectors using a wide range of parameter values for the different processing tasks (Table 1). As there are no simultaneous data of drifter tracks and satellite images for the Gulf of St. Lawrence, this was done using a pair of SST images taken on 21 June 1995 for which a grid of reference vectors was manually built by an experienced operator. The comparisons are thus indicative of the ability of the method to correctly evaluate feature motion and not of computing exact surface currents. The calculated vectors were classified into 10 classes depending on their similarity to the nearest vector in the reference grid. The final selection of the different parameter values also took into

account the quantity of the calculated vectors. A compromise thus had to be made between calculating only a few very good estimated vectors or having a larger number of mostly incorrect vectors. The parameter values retained for the different tasks are shown in Table 1. As they represent an optimum choice for the Gulf of St. Lawrence features, care must be taken before using these values in a different environment.

Table 1. Range and optimum of values used for the different parameters tested.

Task	Parameter	Range tested	Optimum value
Local contrast maximization	Tx1, Ty1	5 to 60	13, 13
Poor image generation filter	K1	1 to 60	5
	K2	0 to 50	2
Rich image generation filter	Tx2, Ty2	5 to 60	25, 25
	K3	1 to 20	8
	K4	0 to 50	12
Image reconstruction	K5	10 to 120	87
Shape-matching	Tx3, Ty3	10 to 80	40, 40
	K6	0 to 1	0.15
Hough transform	Tx3, Ty3	10 to 80	40, 40
	K7	0 to 1	0.51
	K8	0 to 100	10

To test the shape-matching method, we devised a two-step procedure. The first step had the objective to evaluate the precision and sensitivity to noise while the second step is to find the optimum operational parameters. Because simple geometric figures would be too symmetrical, leading to the previously discussed ill-conditioned equation system, the first series of tests was conducted using a feature extracted from a real edge. This feature was made of 146 points and was contained in a 40x40 pixel window. The feature was first transformed using known parameters and the shape-matching method was used to estimate the applied transformations.

Independent tests were made for each of the three possible transformations in order to keep results manageable. First, we tested the translation so that the resulting feature was covered by three different search windows in order to reproduce the operational conditions. Results showed that the similarity criteria did not always correlate well with the precision of the estimation. However, all the imposed translations were estimated accurately at the pixel-precision level. Rotation was tested using the case of a perfect framing of the rotated feature within the search window. The test showed that the angles were precisely estimated with the similarity coefficient being close to unity. For scaling, the tests showed that all applied factors were correctly estimated with the exception of a large expansion of the feature (1.67x). This can be partially explained by the way the tests were devised and is of limited concern since real SST features do not generally expand that much over the typical time frame of less than 12 hours between two analyzed images.

Sensitivity to noise was evaluated in the following manner. Since the features are contained in a binary image (white points over a black background), noise can only take the form of adding (removing) white points in the window. An algorithm was thus built to draw a random coordinate within the window. If this coordinate corresponds to an edge point, the point is withdrawn (made black); if not, a point is added (made white). The signal/noise ratio (S/N) is defined as the ratio of the total number of points in the shape to the number of modified points. For the first test, the starting window contained the original shape while the search window contained a translated shape (5, 0). Noise was only added to the searched image to represent natural feature degradation with time. Results (Table 2) show that the similarity coefficient is consistent with the S/N ratio and that the error on scaling and/or translation becomes important for S/N values less than five. For the second test, the image was both translated (0, 5) and rotated by 29° before noise was added. Results show that once again the similarity coefficient reflects well the effect of added noise and that a S/N level of less than 2.5 leads to incorrect estimates (Table 3). These tests lead us to conclude that in the absence of noise, the motion parameters should be correctly estimated if the shapes analyzed contain a minimum number of points. When noise is present, the estimated parameters should represent reality if the S/N ratio is higher than five.

The second series of tests involved the processing of actual SST images to estimate the optimal algorithm parameters. These include the window size and the similarity coefficient. Tests were performed with the same image pair used for the optimization of the edge detection parameters.

Table 2. Effect of noise on the quality of the shape-matching processing: translation only.

Signal/Noise	Calculated similarity	Scaling error	Rotation error (degrees)	Translation error |x| / °
No noise	1.00	0.00	0.00	0.00 / 0.00
10	0.96	-0.03	0.00	0.33 / -2.70
5	0.79	-0.11	0.57	0.09 / -13.87
2.5	0.76	0.00	2.29	1.97 / 8.91
1.25	0.64	-0.09	0.00	8.47 / 34.29

Using real SST images for these tests implied that we did not control the feature. Also, as in actual operating conditions, features were not perfectly framed and many features could be part of a single tile. These tests should reflect the true performance of the algorithm. To evaluate optimal window size, we conducted a test using the same image for both the start and search images. The algorithm should therefore find vectors reflecting a null motion (no translation or rotation and sizing of 1). Table 4 shows that the proportion of vectors that were correctly evaluated reached a peak for a tile size of 40x40. The use of a smaller tile resulted in many wrong matches while larger tiles identified fewer vectors. To verify this result, a pair of different images was used that reflected operating conditions. Table 5 shows that the highest proportion of good

vectors was generated using a slightly larger window size than with the previous test. However, since the number of good vectors found was roughly the same, we concluded that a size of 40x40 would be optimal. Note that the calculated similarity coefficient was smaller in the real case, showing that the shapes were already deformed during the two hours between the image acquisitions.

Table 3. Effect of noise on the quality of the shape-matching processing: translation plus rotation.

Signal/Noise	Calculated similarity	Scaling error	Rotation error (degrees)	Translation error |x| / °
No noise	1.02	-0.13	1.72	1.26 / 2.75
10	0.95	-0.08	2.87	0.48 / 10.51
5	0.87	-0.07	0.57	1.01 / 5.63
2.5	0.75	-0.08	1.72	1.53 / 7.75
1.25	0.6	-0.11	19.48	5.68 / 42.15
0.625	0.41	-0.30	26.36	10.45 / 47.18

Table 4. Optimization of the shape-matching window size (same image).

Window size (pixels)	Number of vectors	Correctly estimated vectors	Percentage of correctly estimated vectors	Mean similarity
20x20	45	12	27	0.99
30x30	34	12	35	0.97
40x40	25	19	76	0.98
50x50	19	12	63	0.96
60x60	17	10	59	0.97
70x70	17	12	71	0.98
80x80	13	8	69	0.99

Table 5. Optimization of the shape-matching window size (different images).

Window size (pixels)	Number of vectors	Correctly estimated vectors	Percentage of correctly estimated vectors	Mean similarity
20x20	45	6	13	0.95
30x30	28	5	18	0.88
40x40	19	6	32	0.84
50x50	12	6	50	0.82
60x60	11	6	55	0.82
70x70	9	2	22	0.86
80x80	6	1	17	0.72

The last parameter to optimize was the similarity coefficient. The higher the coefficient, the fewer vectors will be kept by the procedure, but they should be of higher quality. The objective, as with the optimization of the other parameters, is to find a compromise between the number of generated vectors and their quality. It appears that a similarity coefficient between 0.85 and 1.15 (similarity parameter K6 equal to 0.15) produced a good number of vectors, most of which were judged correct (Figure 7).

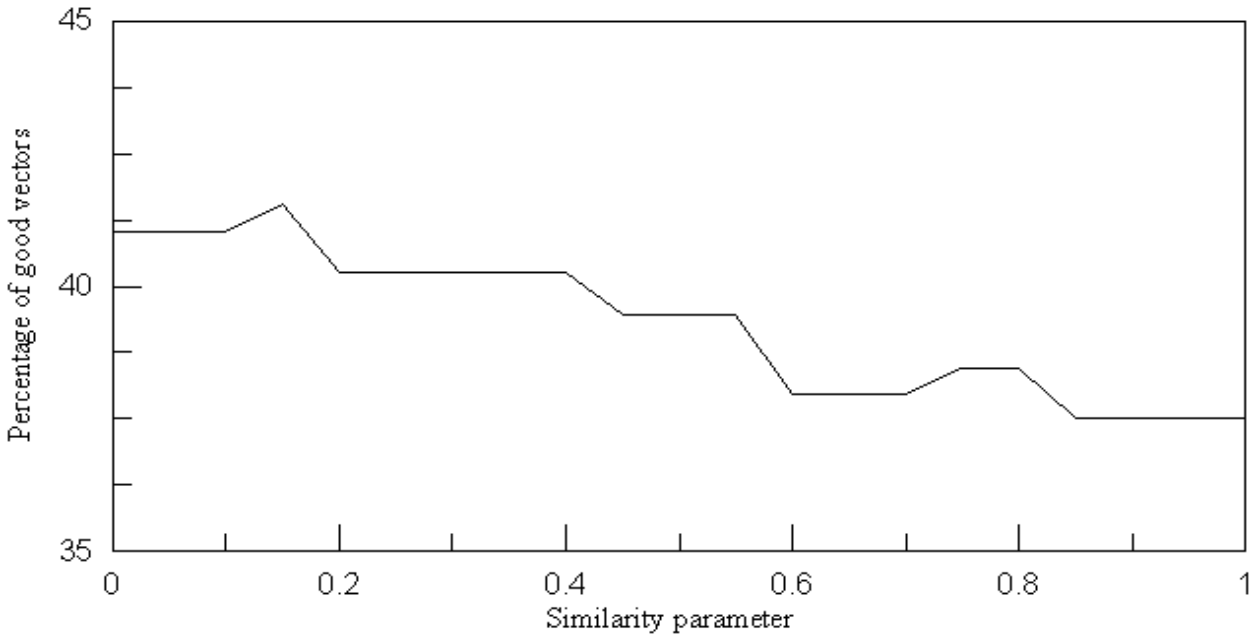

Figure 7. Percentage of good vectors as a function of the similarity parameter.

An in-depth analysis of the different tests showed many defects with the shape-matching approach, the most important one being the insufficient selectivity of the similarity coefficient for this application. Vectors characterized by a similarity of 1 were often totally wrong. These

vectors were the result of a rotation of more than 90° or a scaling of more than 2 while the most probable transformation was a sizing close to 1 and a small rotation. The analysis showed that the right transformation was evaluated by the algorithm but rejected because its similarity was slightly smaller than the anomalous one. Also, in the case of vectors having identical similarity coefficients, the algorithm only kept the last one evaluated. The similarity criterion is based on a ratio of a number of points. This criterion is not sufficiently selective because alternate transformations can yield the same coefficient. We thus defined a set of constraints to address the weaknesses detected during the tests.

The first series of constraints deals with the estimated parameters. Local oceanic conditions indicate that surface currents should not exceed 1.5 m s^{-1}. All calculated vectors above this level are thus eliminated. We also fixed a limit of 20° on the amount of rotation that features could undergo over the typical time scales (1-12 h) considered. Finally, all the tests showed that scale deformations were small. We thus fixed this parameter to be within (0.5, 2).

Finally, as indicated earlier, there is the problem of framing. A starting window may contain only a small number of edge points (or noise) yielding a similarity coefficient close to unity while results will be anomalous. An input parameter setting the minimum number of points within a window is needed. The ideal solution would be to adapt the window size and position to the different shapes that were detected in the first part of the processing, as was done by Kuo and Yan (1994). However, this would lead us to a different set of problems including feature recognition and labelling. Instead of finding the best framing possible, we excluded the worst ones. This new constraint requires that a shape in the starting window have its geometric center within a square centered on the reference point and of size (Tx3/2, Ty3/2), eliminating small portions of edges that could appear in a window.

Tests showed that adding constraints reduced the total number of vectors by at least half. However, the ratio of good vectors was significantly higher, now exceeding 80%. The number of vectors considered to be correct was thus reduced but their reliability was increased.

Tests were done in order to evaluate results obtained using the Hough transform. First, we took the same single natural feature that was used in section 3.2 for the shape matching tests and transformed it using a translation of (5, 2), a rotation of -17° and sizing of 0.8. We then used the two algorithms (Hough transform alone; shape-matching and Hough transform together) to evaluate the motion. The best result was obtained by the second approach combining the strength of both the shape-matching and Hough transform (Table 6). The Hough transform alone provides inadequate results because of its inability to evaluate rotation and sizing.

Further tests were done to verify if the addition of a polar constraint on the Hough transform would provide better results. That transformation generates an intrinsically noisy accumulator array with many peaks that can affect the detection of the real maximum. This noise can be reduced by putting in correspondence only the points in both images that have approximately the same gradient direction. However, results showed that this new constraint did not affect the results significantly. This is probably the result of the shape-matching pre-processing step that already orients the direction of the feature to be found in the search window.

Table 6. Performance of the motion evaluation methodologies.

	Real transformation	Hough transform	Shape-matching + Hough transform
Rotation (°)	-17	-20	-14.9
Sizing	0.8	-	0.81
Translation (pixels)	(5, 2)	(7.99, 2.01)	(5.02, 2.0)

3.3 SYSTEM PERFORMANCE

Finally, tests were done using a larger set of 19 image pairs representing operating conditions. The images used were separated by different periods (1.5 to 15.5 hours) and taken at different seasons of the year (May, June and August). This was done to evaluate the effect of SST contrast and shape modification on system performance and to verify that the parameters were not overly adapted to the image pair that was used to optimize them. It was found that the most important problem affecting the quality of the results was cloud contamination of the images. Small clouds or fog not detected by the masking procedure generate transient features that were processed by the system as true edges generating false vectors and lowering the overall system performance. For the 19 image pairs processed, the mean percentage of vectors found to be related to this problem was 41% (with a standard deviation of 24%). These vectors were eliminated from the final results.

As the image pair used to optimize the different parameters was included in the system performance tests (#12), it was possible to evaluate if these parameters were too adapted to it. Figure 8 shows the percentage of good vectors for the 19 image pairs used. Results show that pair #12 was among the four highest values, which may indicate some kind of optimization. However, another important factor affecting the quality of the results must also be taken into account when comparing the performance of the system. Despite a large amount of scatter, Figure 9 shows that the time separation between images has a significant effect on the proportion of generated good vectors, with the bests results obtained when the time difference is small. Comparing the results for pair #12 with those of pair #4 which has an identical time difference, shows a difference in the percentage of good vectors of 12% in favour of pair #12. This also supports the idea that the different parameters could be adapted to the particular image pair used to optimized the parameters. However, other pairs having about the same time difference also show large variations in the percentage of good vectors generated (e.g., pairs 1, 7, 9, and 19). This shows that the results are dependent on a large number of factors that can affect their quality (e.g., the quality of the features, the small number of vectors found, the feature displacement, the location of the features in the Gulf, the quality of the image registration, the effect of day vs night images). With the relatively small number of image pairs processed, it is thus hard to evaluate if

the optimization process was overly adapted to its image pair. We however believe that the parameter values found should generate relatively good results in most situations.

The best results were generally obtained when the image pairs were separated by a small amount of time (Figure 9). This is consistent with previous experiments showing that better results are obtained for smaller time difference between the images (Tokmakian et al. 1990; Kelly and Strub 1992). The time limit to get a satisfactory number of good vectors (about 50%) appears to be around 6 hours, with the best results obtained using data from consecutive NOAA passes (~100 minutes). This small time delay also reduces the problems associated with thermal diffusion of the tracked features. With such a level of good vectors, it should be possible to apply a post-processing filtering scheme that would eliminate remaining bad vectors based on knowledge of the ecosystem using criteria such as the spatial continuity of the vectors (Pope and Emery 1994; Domingues et al. 2000; Bowen et al. 2002) or simply calculating mean vectors using multiple consecutive pairs to reduce the uncertainty (Kelly and Strub 1992; Emery et al. 2004; Navarro et al. 2004). The set of remaining vectors can then be processed using methods such as optimal interpolation (Emery and Thomson 1998) to provide an estimate of surface movement over the entire domain. An alternate choice to post-processing would be to use a set of much stricter parameters to generate a handful of very reliable vectors. The drawback to this approach is that more images will be needed to characterize surface circulation over an area.

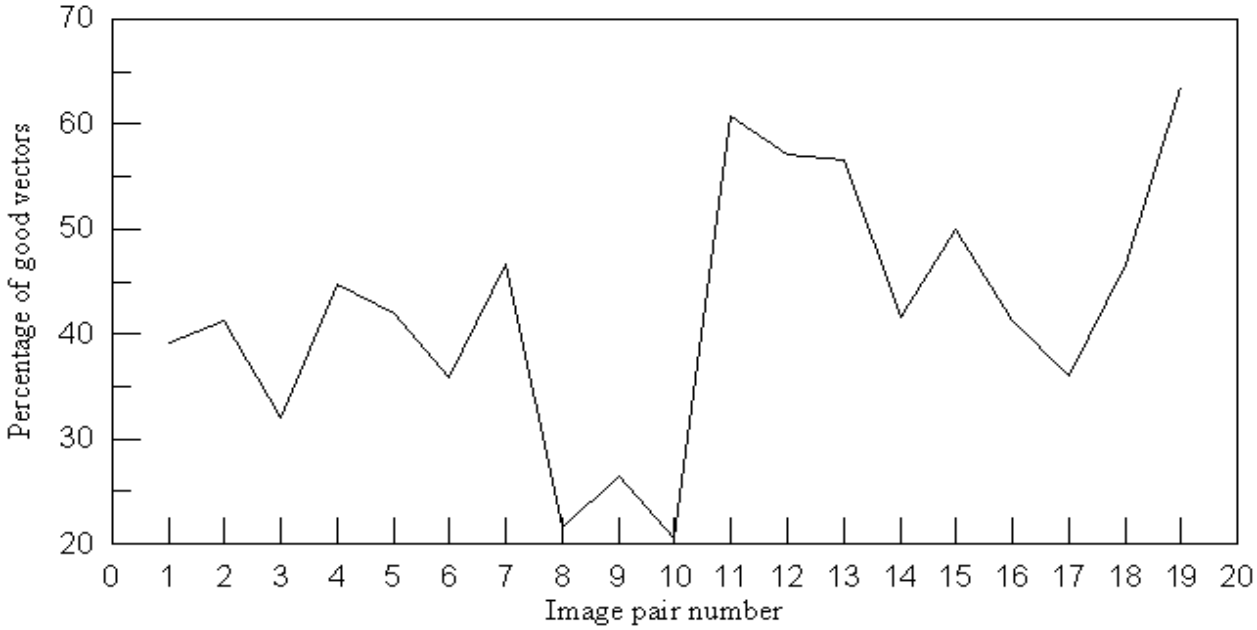

Figure 8. Percentage of good vectors for the 19 image pairs used.

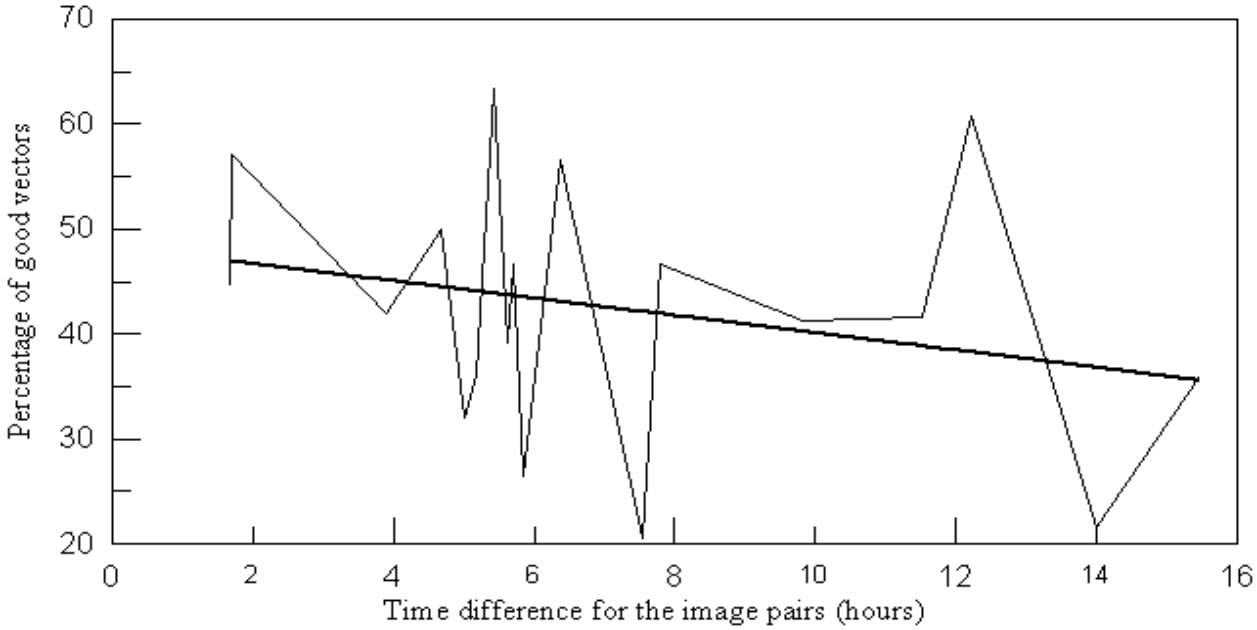

Figure 9. Percentage of good vectors as a function of the time difference between the two images used. The line in bold shows the trend in the series.

4.0 DISCUSSION

This report presents the development of a system to measure sea surface feature motion for the Gulf of St. Lawrence region. The system comprises a relatively large number of processing steps, all of which can affect the accuracy of feature motion tracking to various degrees. In our opinion, the most critical steps in the process are the cloud masking procedure and the feature identification. All the other steps appear to be less problematic. Cloud masking is a problem that is not addressed specifically in this paper but for which much has been done in the past (Maturi and Pichel 1994; Sølvsteen 1995; Cayulla and Cornillon 1996; Jones et al. 1996; Shin et al. 1996; Stowe et al. 1999; Kärner and Di Girolamo 2001; Simpson et al. 2001). The better the cloud masking is, the better the automated process will perform as less noise will propagate through the system. The Gulf of St. Lawrence does not appear to be a particularly difficult place to do cloud masking, so algorithms developed elsewhere should perform reasonably well, with outliers eventually picked up and eliminated by post-processing.

The second critical component of the system is feature identification. The better the features are identified and framed, the better the results are. As described earlier, the system includes tests to identify and eliminate objects that were not deemed adequate for feature tracking. More work could be done in this direction to further develop the feature identification process, but as a first step, the current system performs well enough to warrant its use.

One of our long-term goals was to be able to use the system in other environments. Even though the different parameters were optimized for the Gulf of St. Lawrence region, we believe that the system could probably be used in other environments without much change since the Gulf of St. Lawrence encompasses many sub-regions with a large diversity of oceanographic characteristics.

The choices made for the 12 parameters thus reflect an overall ability to operate in all these conditions.

The proposed system is a new step in the development of automatic feature tracking for the open sea. Until now, most algorithms have been developed as a demonstration of possibilities using only a few image pairs and without quantitatively characterizing their performances. Even if there are limitations to its use, only the maximum cross-correlation algorithm has been applied for the processing of relatively large amounts of images (Bowen et al. 2002) and has been used in an operational context (ccar.colorado.edu/research/cali/index.html; last accessed August 16, 2006) on the US East and West coasts.

What we are proposing is not just a new feature-tracking method, but an integrated system combining the strengths of the shape-matching and the Hough transform. All system components were thoroughly tested and their performance evaluated in a real-world application leading to the definition of optimal parameters for the Gulf of St. Lawrence region. In particular, efforts were made to evaluate the system sensitivity to the identification of features, which has never been done before. The system thus integrates a better way to define features using mathematical morphology operators instead of gradient images used without post-processing. It is true that, compared to the MCC method, the system does not generate large amounts of information from a single pair of images and that the generated vector reliability is around 50%. Its application to generate real-time motion data is also limited without post-processing of the results. However, the system was developed with the objective to study mean circulation patterns. Processing a large number of images can therefore lead to that goal.

5.0 CONCLUSION

Our objective was to develop a robust processing system to extract ocean surface circulation information from thermal infrared satellite data over the Gulf of St. Lawrence. The multiple tests done showed that many factors can influence the quality of the results. The developed system integrates many criteria to ensure that this quality is sufficient. The number of good estimations on each image may appear small, but it is larger than any drifter program done in the St. Lawrence in the past. By processing a large number of images and developing a post-processing system capable of qualifying the produced vectors, we should be able to characterize the general circulation patterns in the Gulf of St. Lawrence. The system can be easily implemented and only uses a small amount of CPU time (6 min to analyze a pair of 1152x736 images using a 100 mips, 128 Mb memory workstation). The system was shown to work with images representing areas of different dynamics, allowing its use year-round under open-water conditions.

6.0 ACKNOWLEDGEMENTS

This work was supported by a grant from the Université des Réseaux d'Expression Française (UREF). Thanks to Peter Galbraith, Denis Gilbert and Laure Devine for providing useful comments to earlier versions of this report.

7.0 REFERENCES

Bowen, M. M., Emery, W. J., Wilkin, J. L., Tildesley, P. C., Barton, I. J. and Knewtson, R. 2002. Extracting multiyear surface currents from sequential thermal imagery using the maximum cross-correlation technique. Journal of Atmospheric and Oceanic Technology, 19: 1665-1676.

Boxall, S. R. and Robinson, I. S. 1987. Shallow sea dynamics from CZCS imagery. Advances in Space Research, 7: 37-46.

Cayula, J.-F. and Cornillon, P. 1996.Cloud detection from a sequence of SST images. Remote Sensing of Environment, 55: 80-88.

Cho, E. C., Iyengar, S. S., Seetharaman, G., Holyer, R. J. and Lybanon, M. 1998. Velocity vectors for features of sequential oceanographic images. IEEE Transactions on Geoscience and Remote Sensing, 36: 985-998.

Côté, S. and Tatnall, A. R. L. 1995. A neural network-based method for tracking features from satellite sensor images. International Journal of Remote Sensing, 16: 3695-3701.

Domingues, C. M., Gonçalves, G. A., Ghisolfi, R. D. and Garcia, C. A. E. 2000. Advective surface velocities derived from sequential infrared images in the Southwestern Atlantic ocean. Remote Sensing of Environment, 73: 218-226.

Emery, W. J. and Thomson, R. E. 1998. Data analysis methods in physical oceanography. Pergamon, New York, USA, 634 pp.

Emery, W. J., Thomas, A. C., Collins, M. J., Crawford, W. R. and Mackas, D. L. 1986. Comparison between satellite image advective velocities, dynamic topography, and surface drifter trajectories. Eos, 67: 498-499.

Emery, W. J., Fowler, C. and Clayson, A. 1992. Satellite-image-derived Gulf Stream currents compared with numerical model results. Journal of Atmospheric and Oceanic Technology, 9: 286-304.

Emery, W., Matthews, D., Crocker, R. and Baldwin, D. 2004 Surface current mapping off California with radiometry and altimetry. Gayana (Concepción), 68 (supp): 174-179.

Gao, J. and Lythe, M. B. 1998. Effectiveness of the MCC method in detecting oceanic circulation patterns at a local scale from sequential AVHRR images. Photogrammetric Engineering and Remote Sensing, 64: 301-308.

Garcia, C. A. E. and Robinson, I. S. 1989. Sea surface velocities in shallow seas extracted from sequential coastal zone color scanner satellite data. Journal of Geophysical Research, 94: 12681-12691.

Hatakeyama, Y., Tanaka, S., Sugimura, T. and Nishimura, T. 1985. Surface currents around Hokkaido in the late fall of 1981 obtained from analysis of satellite images. Journal of the Oceanographic Society of Japan, 41: 327-336.

Hedger, R. D., Malthus, T. J. and Folkard, A. M. 2001. Estimation of velocity fields at the estuary - coastal interface through statistical analysis of successive airborne remotely sensed images. International Journal of Remote Sensing, 22: 3901-3906.

Holland, J. A. and X.-H. Yan 1992. Ocean thermal feature recognition, discrimination and tracking using infrared satellite imagery. IEEE Transactions on Geoscience and Remote Sensing, 30: 1046-1053.

Holyer, R. J. and Peckinpaugh, S. H. 1989. Edge detection applied to satellite imagery of the oceans. IEEE Transactions on Geoscience and Remote Sensing, 27: 46-56.

Jones, M. S., Saunders, M. A. and Guymer, T. H. 1996. Reducing cloud contamination in ATSR averaged sea surface temperature data. Journal of Atmospheric and Oceanic Technology, 13: 492-506.

Kamachi, M. 1989. Advective surface velocities derived from sequential images for rotational flow field: Limitations and applications of maximum cross-correlation method with rotational registration. Journal of Geophysical Research, 94: 18227-18233.

Kärner, O. and Di Girolamo, L. 2001. On automatic cloud detection over ocean. International Journal of Remote Sensing, 22: 3047-3052.

Kelly, K. 1989. An inverse model for near-surface velocity from infrared images. Journal of Physical Oceanography, 19: 1845-1864.

Kelly, K. A. and Strub, P. T. 1992. Comparison of velocity estimates from advanced very high resolution radiometer in the coastal transition zone. Journal of Geophysical Research, 97: 9653-9668.

Kohler, R. 1981. A segmentation system based on thresholding. Computer Graphics and Image Processing, 15: 319-338.

Krishnamurthy, S., Sitharama Iyengar, S., Holyer, R. J. and Lybanon, M. 1994. Histogram-based morphological edge detector. IEEE Transactions on Geoscience and Remote Sensing, 32: 759-767.

Kuo, N.-J. and Yan, X.-H. 1994. Using the shape-matching method to compute sea-surface velocities from AVHRR satellite images. IEEE Transactions on Geoscience and Remote Sensing, 32: 724-728.

LaViolette, P. E. and Hubertz, J. M. 1975. Surface circulation patterns off the east coast of Greenland as deduced from satellite photographs of ice floes. Geophysical Research Letters, 2: 400-402.

Lee, J. S. 1984. Edge detection partitioning. *In* Statistical Image Processing. Edited by E. G. Wegman and J. G. Smith. New York, Dekker, pp. 59-69.

Leming, T. D. 1994. Hierarchical estimation of surface velocity fields from satellite imagery. *In* Proceedings of the second thematic conference on remote sensing for marine and coastal environments. Ann Arbor, USA, Environmental Research Institute of Michigan, I677-I678.

Maturi, E. M. and Pichel, W. G. 1994. Cloud masking for Coastwatch satellite imagery. *In* Proceedings of the seventh conference on satellite meteorology and oceanography. Monterey, California, USA, pp. 569-573.

Navarro, E., Schneider, W. and Letelier, J. 2004. Estimation of onshore-offshore transport off central Chile by means of maximum cross-correlation using satellite derived SST. Gayana (Concepción), 68 (supp): 427-431.

Peterson, I. 1987. A snapshot of the Labrador Current inferred from ice-floe movement in NOAA satellite imagery. Atmosphere-Ocean, 25: 402-415.

Pope, P. A. and Emery, W. J. 1994. Sea surface velocities from visible and infrared Multispectral Atmospheric Mapping Sensor (MAMS) imagery. IEEE Transactions on Geoscience and Remote Sensing, 32: 220-223.

Shin, D., Pollard, J. K. and Muller, J.-P. 1996. Cloud detection from thermal infrared images using a segmentation technique. International Journal of Remote Sensing, 17: 2845-2856.

Simpson, J. J., McIntire, T. J., Stitt, J. R. and Hufford, G. L. 2001. Improved cloud detection in AVHRR daytime and night-time scenes over the ocean. International Journal of Remote Sensing, 22: 2585-2615.

Sølvsteen, C. 1995. A correlation based cloud-detection algorithm combined with an examination of some split-window assumptions. International Journal of Remote Sensing, 16: 2875-2901.

Stowe, L. L., Davis, P. A. and McClain, E. P. 1999. Scientific basis and initial evaluation of the CLAVR-1 global clear/cloud classification algorithm for the advanced very high resolution radiometer. Journal of Atmospheric and Oceanic Technology, 16: 656-681.

Svejkovsky, J. 1988. Sea surface flow estimation from Advanced Very High Resolution Radiometer and Coastal Zone Color Scanner satellite imagery: a verification study. Journal of Geophysical Research, 93: 6735-6743.

Thomas, J. P., Turner, J., Lachlan-Cope, T. A. and Corcoran, G. 1995. High resolution observations of Weddel Sea surface currents using ERS-1 SAR sea-ice motion vectors. International Journal of Remote Sensing, 16: 3409-3425.

Tokmakian, R., Streb, P. T. and McClean-Padman, J. 1990. Evaluation of the maximum cross-correlation method of estimating sea surface velocities from sequential satellite images. Journal of Atmospheric and Oceanic Technology, 7: 852-865.

Tonsmann, G., Tyler, J. M., Walker, N. D., Rouse, L. and Wiseman, W. J. 2002. A multiresolution algorithm for the estimation of oceanic surface velocity vector fields. *In* Proceedings of the 7th International Conference on Remote Sensing for Marine and Coastal Environments. Miami, USA, Veridian International. CD-ROM.

Vastano, A. C. and Barron Jr, C. N. 1994. Comparison of satellite and drifter surface flow estimates in the northwestern gulf of Mexico. Continental Shelf Research, 14: 589-605.

Vigan, X., Provost, C., Bleck, R. and Courtier, P. 2000. Sea surface velocities from sea surface temperature image sequences. 1. Method and validation using primitive equation model output. Journal of Geophysical Research, 105: 19499-19514.

Wahl, D. D. and Simpson, J. J. 1990. Physical processes affecting the objective determination of near-surface velocity from satellite data. Journal of Geophysical Research, 95: 13511-13528.

Yan, X.-H. and Breaker, L. C. 1993. Surface circulation estimation using image processing and computer vision methods applied to sequential satellite imagery. Photogrammetric Engineering and Remote Sensing, 59: 407-413.